ACCOUNTS
of chemical research

Bioprobes Based on AIE Fluorogens

DAN DING,[†] KAI LI,[‡] BIN LIU,[*,†,‡] AND BEN ZHONG TANG[*,‡,§,∥]

[†]*Department of Chemical and Biomolecular Engineering, National University of Singapore, 4 Engineering Drive 4, Singapore 117576,* [‡]*Institute of Materials Research and Engineering, 3 Research Link, Singapore 117602,* [§]*Department of Chemistry, Institute for Advanced Study, Division of Biomedical Engineering, State Key Laboratory of Molecular Neuroscience, and Institute of Molecular Functional Materials, The Hong Kong University of Science & Technology, Clear Water Bay, Kowloon, Hong Kong, China, and* [∥]*SCUT−HKUST Joint Research Laboratory, Guangdong Innovative Research Team, State Key Laboratory of Luminescent Materials and Devices, South China University of Technology, Guangzhou 510640, China*

RECEIVED ON DECEMBER 21, 2012

CONSPECTUS

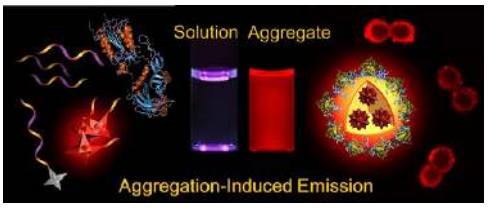

Fluorescent bioprobes are powerful tools for analytical sensing and optical imaging, which allow direct visualization of biological analytes at the molecular level and offer useful insights into complex biological structures and processes. The sensing and imaging sensitivity of a bioprobe is determined by the brightness and contrast of its fluorescence before and after analyte binding. Emission from a fluorophore is often quenched at high concentration or in aggregate state, which is notoriously known as concentration quenching or aggregation-caused quenching (ACQ). The ACQ effect limits the label-to-analyte ratio and forces researchers to use very dilute solutions of fluorophores. It compels many probes to operate in a fluorescence "turn-off" mode with a narrow scope of practical applications.

The unique aggregation-induced emission (AIE) process offers a straightforward solution to the ACQ problem. Typical AIE fluorogens are characterized by their propeller-shaped rotorlike structures, which undergo low-frequency torsional motions as isolated molecules and emit very weakly in solutions. Their aggregates show strong fluorescence mainly due to the restriction of their intramolecular rotations in the aggregate state. This fascinating attribute of AIE fluorogens provides a new platform for the development of fluorescence light-up molecules and photostable nanoaggregates for specific analyte detection and imaging.

In this Account, we review our recent AIE work to highlight the utility of AIE effect in the development of new fluorescent bioprobes, which allows the use of highly concentrated fluorogens for biosensing and imaging. The simple design and fluorescence turn-on feature of the molecular AIE bioprobes offer direct visualization of specific analytes and biological processes in aqueous media with higher sensitivity and better accuracy than traditional fluorescence turn-off probes. The AIE dot-based bioprobes with different formulations and surface functionalities show advanced features over quantum dots and small molecule dyes, such as large absorptivity, high luminosity, excellent biocompatibility, free of random blinking, and strong photobleaching resistance. These features enable cancer cell detection, long term cell tracing, and tumor imaging in a noninvasive and high contrast manner. Recent research has significantly expanded the scope of biological applications of AIE fluorogens and offers new strategies to fluorescent bioprobe design. We anticipate that future development on AIE bioprobes will combine one- or multiphoton fluorescence with other modalities (e.g., magnetic resonance imaging) or functionalities (e.g. therapy) to fully demonstrate their potential as a new generation of theranostic reagent. In parallel, the advances in molecular biology will provide more specific bioreceptors, which will enable the development of next generation AIE bioprobes with high selectivity and sensitivity for molecular sensing and imaging.

1. Introduction

Researchers are in enthusiastic pursuit of fluorescent bioprobes as they allow direct visualization of bioanalytes on site and in time and offers useful insights into complex biological structures and processes.[1] High selectivity and sensitivity are the primary requirements for a fluorescent bioprobe to be practically useful. The selectivity is largely determined by the affinity between specific recognition

Published on the Web 06/06/2013 www.pubs.acs.org/accounts
10.1021/ar3003464

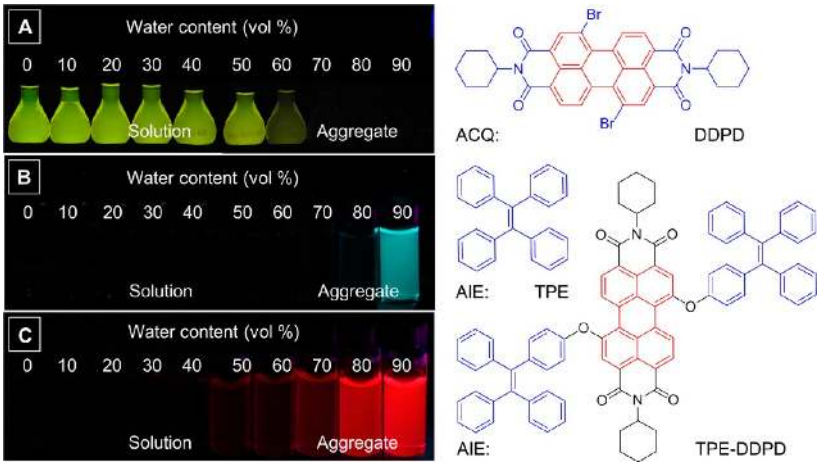

FIGURE 1. Fluorescence photographs of (A) DDPD with aggregation-caused quenching (ACQ) feature and (B) TPE and (C) TPE-DDPD with aggregation-induced emission (AIE) attribute in THF/water mixtures with different water contents upon UV illumination.

elements and receptors, while the sensitivity is usually dependent on the brightness of the probe fluorescence and the contrast between the emissions before and after the probe binding to an analyte.

Light emissions from conventional fluorophores are often quenched at high concentrations or in aggregate state, which is known as concentration quenching or aggregation-caused quenching (ACQ).[2] The ACQ effect has also been observed in inorganic luminophores, such as quantum dots (QDs).[3] The notorious ACQ effect has greatly limited the labeling degrees of fluorophores to bioanalytes and forces researchers to use dilute solutions of probes for biosensor applications, leading to significantly compromised sensitivity and posing a formidable hurdle to trace analysis of biomolecules.[4] Even in the dilute solutions, ACQ effect may still be operative, because the bioprobes tend to accumulate on the surfaces of the biomolecules or cluster in their hydrophobic cavities to significantly increase the local probe concentrations and hence quench their emissions. The ACQ effect has compelled many fluorescent probes to operate in a fluorescence "turn-off" mode with a limited scope of practical applications.

A typical example of ACQ effect is shown in Figure 1A. The dilute tetrahydrofuran (THF) solution of *N*,*N*-dicyclohexyl-1,7-dibromo-3,4,9,10-perylenetetracarboxylic diimide (DDPD) is highly emissive under UV illumination. The fluorescence is weakened upon addition of water and is diminished when the water fraction (f_w) reaches 70%. Because DDPD has a disclike perylene core, strong $\pi-\pi$ stacking interaction in the aggregate state promotes excimer formation, leading to the observed ACQ effect. Such behavior has been widely observed in conventional fluorophore systems, especially in amphiphilic far-red/near IR (FR/NIR) emitters as they often contain large hydrophobic aromatic rings, which are prone to aggregate in aqueous media and solid state.[5] To mitigate the ACQ effect, various chemical, physical, and engineering approaches have been taken. However, only limited success has been achieved because these approaches work against the natural tendency of aggregate formation of the fluorophores.[6]

We have recently discovered a group of fluorogenic molecules that are nonemissive when molecularly dissolved but highly emissive when aggregated.[7] We coined aggregation-induced emission (AIE) for the observed phenomenon and proposed the restriction of intramolecular rotations (RIR) as its main cause.[6−8] The AIE phenomenon is generally observed in molecules with rotating units such as phenyl rings. The rotor-containing fluorogens undergo low-frequency motions in dilute solutions, causing fast nonradiative decay of the excited states that makes the fluorogens nonemissive. In the aggregates, these motions are blocked by intermolecular steric interaction, which opens the radiative pathway. Taking hexaphenylsilole (HPS) as an example, it shows spectral characteristics distinctly different from those of the fluorophores containing donor−acceptor units that can form J- or H-aggregates. From molecular to aggregative state, HPS does not exhibit spectral shift or solvatochromic effect, whereas obvious shift in the absorption maximum with weakened fluorescence are often observed for the later upon aggregate formation or increasing solvent polarity. Detailed discussions on the RIR mechanism and various AIE systems can be found in our recent reviews.[6,9]

Tetraphenylethylene (TPE) is an iconic AIE fluorogen: it is nonfluorescent in THF solution but becomes emissive in a

CHART 1. Scope of this Account: Bioprobes Based on AIE Fluorogens

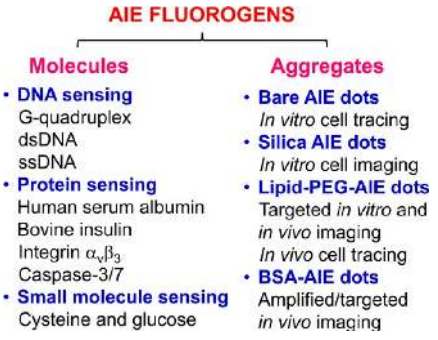

THF/water mixture with high f_w, where its molecules aggregate (Figure 1B). Its simple structure makes it an ideal model for construction of various fluorescent sensors.[6,10] Our recent discovery that melding AIE units with conventional ACQ units (AIE + ACQ) can effectively transform ACQ fluorophores into AIE fluorogens has further enriched AIE systems with emissions from blue to red.[9] The miracle is illustrated in Figure 1C. Attachment of two TPE pendants to a DDPD skeleton yields a TPE-DDPD adduct with a marked AIE activity. TPE-DDPD emits faintly in a THF solution but intensely in a THF/water mixture with f_w of 90%.[11] The smart molecular transformation strategy has been proved general and effective in synthesizing FR/NIR AIE fluorogens through conjugations of TPE with other AIE units (AIE + AIE)[12] or chromophores with twisted intramolecular charge transfer characteristics (AIE + TICT).[13,14] These examples demonstrate that the AIE strategy based on harnessing aggregation process is able to preserve excellent functional properties of the components and solve the ACQ problem without causing adverse effects. The weak and strong emissions from AIE molecules and aggregates, respectively, offer unprecedented opportunities for fluorescent probe design.

In this Account, we summarize recent research efforts on the development of AIE *molecules* for fluorescence turn-on biomolecule detection and AIE *aggregates* for in vitro and in vivo tumor cell sensing and imaging (Chart 1). Due to the space limitation, the discussion is limited to our own work from 2010, with the hope to stimulate new ideas and inspire new endeavors in this emerging area of research.

2. Fluorescent Sensing

2.1. DNA Sensing. A single-stranded DNA (ssDNA) sequence with guanine (G)-rich repeat sequences can form a secondary structure known as G-quadruplex that can be further stabilized by monovalent cations (e.g., K^+). As the formation of quadruplex can affect gene expression and inhibit telomerase activity in cancer cells, detection of G-quadruplex is of great importance for designing quartet-specific medication and telomere-aimed anticancer therapeutics. A series of cationic TPE derivatives (**1**−**4** in Figure 2) with weak fluorescence were designed to detect G-quadruplex in solution, among which **1** showed the best performance to G-quadruplex structures formed by human telomeric DNA sequences due to the perfect structural match.[15] In addition, **1** responds to DNA conformational variations. Upon addition of ssDNA (HG21) into the aqueous solution of **1**, the intramolecular rotations in **1** are restricted due to its electrostatic interaction with the HG21 chain and the solution fluorescence is turned on with an emission maximum at 470 nm. G-quadruplex formation is induced upon addition of K^+ ions, resulting in a red-shifted emission at 492 nm. Molecular modeling reveals that **1** docks on the surface of the folding structure of DNA to turn on the fluorescence. Hybridization of HG21 with a complementary ssDNA (C21) unfolds the quadruplex to give double-stranded DNA (dsDNA). As the binding between **1** and dsDNA is greatly suppressed by the competition from K^+ ions, the molecules of **1** are dissociated from the DNA chain to give weak fluorescence. The distinct fluorescence of **1** in the presence of G-quadruplex allows label-free visual detection of G-quadruplex from other DNA conformations with a detection limit of 0.5 μM, which is beneficial to the high-throughput quadruplex-targeting anticancer drug screening and K^+ ion sensing.

While the fluorescence turn-on response makes the cationic AIE fluorogens promising for label-free DNA structure differentiation, the assay selectivity remains an issue as the fluorogens also respond to other biomacromolecules such as RNA and proteins.[6,16] To improve the assay selectivity, a cationic silole derivative (**5**) was used together with graphene oxide (GO) to develop a replacement assay for dsDNA sensing. As a single layer carbon-based nanomaterial, GO is readily dispersed in aqueous media and binds selectively to ssDNA against dsDNA via hydrophobic interaction. GO is able to effectively quench the emission of **5** upon complexation. As calf-thymus DNA (ct-DNA) has a higher binding affinity to **5** than GO, addition of ct-DNA into the GO/**5** complex is able to induce **5**/ct-DNA complexation to light up its fluorescence in solution (Figure 3). In sharp contrast, the GO/**5** complex remains nonemissive after addition of other biomolecules. The blue-greenish fluorescence of **5** in the presence of ct-DNA allows visual discrimination of ct-DNA from other bioanalytes, with a detection limit of 3.3 μg mL^{-1} (Figure 3B). As **5** itself shows

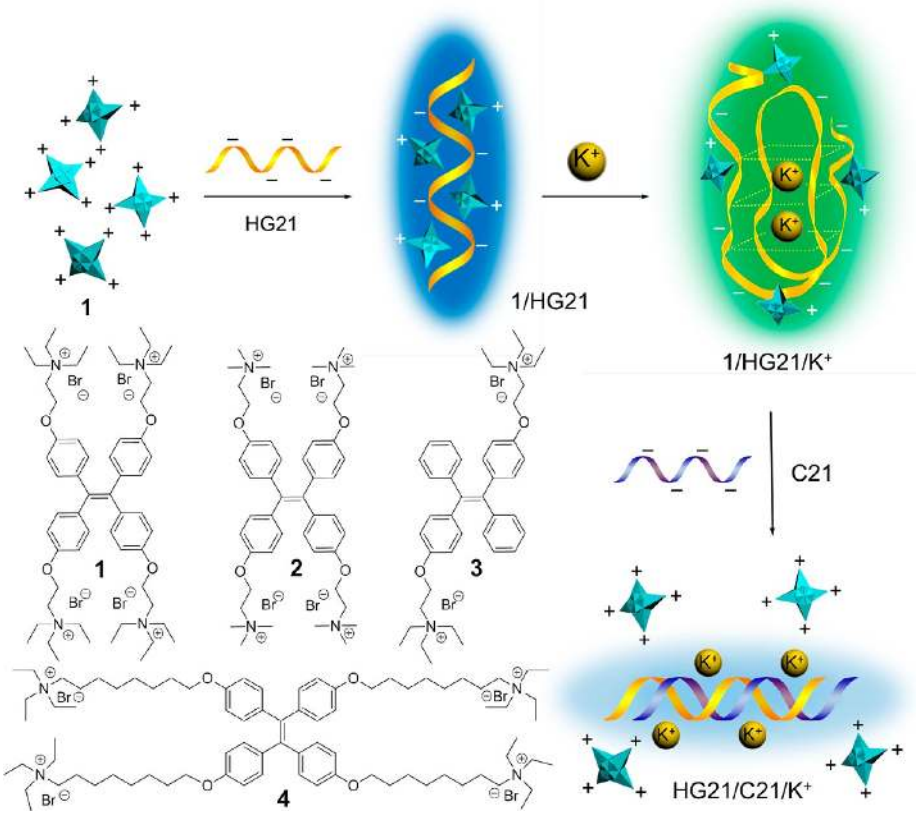

FIGURE 2. Chemical structures of **1**–**4** and schematic illustration of differentiation of DNA conformations by **1**.

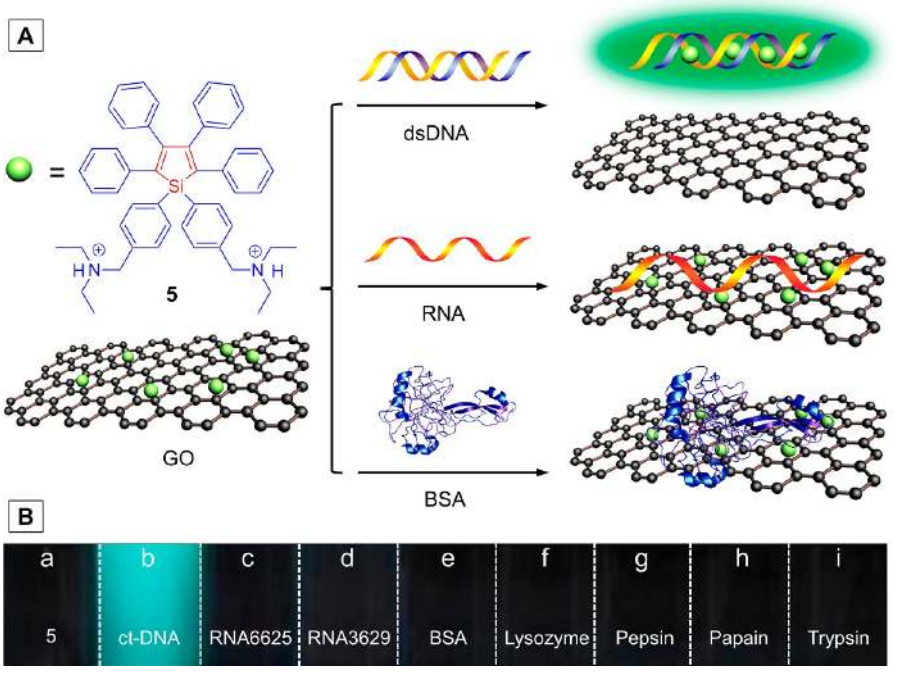

FIGURE 3. (A) Schematic illustration of selective detection of dsDNA by **5** with the aid of GO. (B) Photographs of **5** (a) in solution and (b–i) upon complexation with different biomolecules under UV illumination.

almost no selectivity toward these biomolecules, the results highlight the essential role of GO in transforming an AIE fluorogen into an efficient dsDNA probe with high specificity.

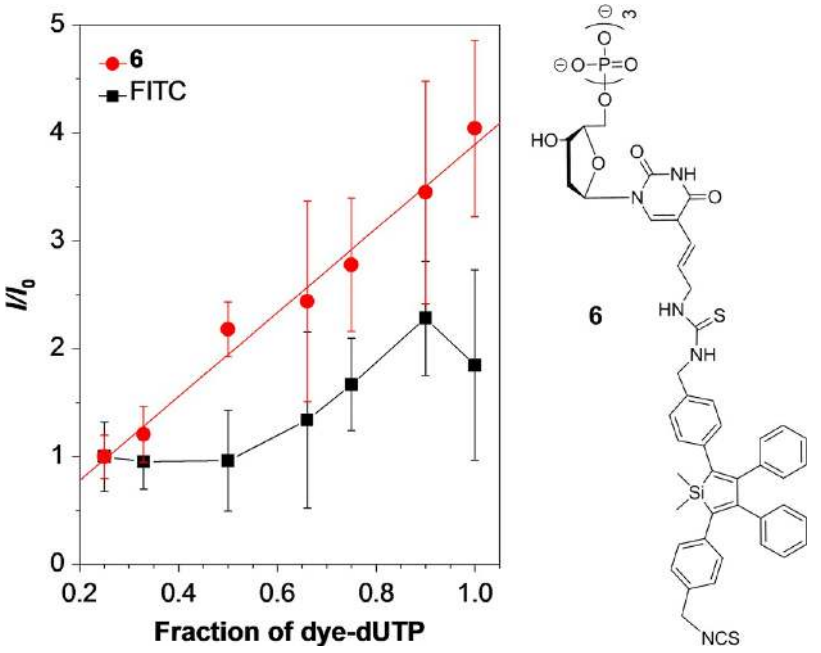

FIGURE 4. Plot of normalized fluorescence intensity of the fluorescent DNA versus fraction of dye-dUTP. I_0 is the fluorescence intensity of the DNA prepared with fraction of dye-dUTP/(dye-dUTP + dTTP) = 0.25. Reproduced with permission from ref 17. Copyright 2012 Royal Society of Chemistry.

To accomplish high DNA detection sensitivity, fluorescent bioprobes with high brightness are required. However, the degree of labeling (DOL), expressed as the number of dyes per 100 bases, must be carefully controlled at a relatively low level to avoid intrinsic ACQ effect of traditional fluorophores. In this regard, using AIE fluorogen-labeled dNTPs for fluorescent nucleic acid synthesis is promising to improve DOL without self-quenching effect. Conjugation of an isothiocyanate-functionalized tetraphenylsilole (TPS) with an amine-modified dUTP leads to fluorescent dUTP **6** with AIE signature, which has been enzymatically incorporated into DNA with high labeling efficiency.[17] The DOL values of the products from **6** and dUTPs are comparable or higher than those from fluorescein isothiocyanate (FITC)-labeled dUTPs through different methods. The fluorescence intensities of the obtained DNA sequences increase linearly upon increasing the percentage of **6** and reach the highest value at 100% of dUTPs, whereas the FITC-labeled DNAs show obvious quenching effect, especially at the high percentage of FITC-dUTPs (Figure 4). As such, incorporation of AIE fluorogen-labeled dUTPs during DNA synthesis provides a direct and feasible method to realize bright fluorescent nucleic acid probes with high sensitivity.

2.2. Protein Sensing. Similar to the light-up response of cationic AIE fluorogens to DNAs, anionic AIE fluorogens (e.g., **7** in Figure 5) light up in the presence of proteins (e.g., human serum albumin, HSA) via both electrostatic and hydrophobic interactions.[6] The capability of **7** to monitor conformational changes of specific proteins was studied using HSA as an example. In a PBS buffer, **7** shows a significant fluorescence increase in response to HSA, with a detection limit of 1 nM.[18] To monitor the conformational change of HSA, different amounts of guanidine hydrochloride (GndHCl) are added to induce HSA unfolding. Fluorescence resonance energy transfer (FRET) from tryptophan residues of HSA to bound **7** allows continuous monitoring of the change in I_{475}/I_{350} during the GndHCl titration, revealing that HSA unfolding occurs in a stepwise fashion with a three-step transition involving a molten-globule intermediate (Figure 5). Similar results were also obtained using anthracene based AIE fluorogens.[19]

Protein misfolding and aggregation into amyloidal fibrils can potentially lead to biological dysfunctions. Real-time monitoring and mechanistic understanding of the amyloid deposition processes are of importance to diagnostics and therapeutics. As insulin can readily undergo the fibrosis process, it was used as a model to study protein amyloidogenesis. As shown in Figure 6A, the fluorescence of **7** is significantly boosted upon mixing with fibrillar insulin in PBS buffer, while being silent to native bovine insulin.[20] The sensitive response of **7** toward insulin allows ex situ monitoring of amyloidogenesis kinetics, revealing a three-stage

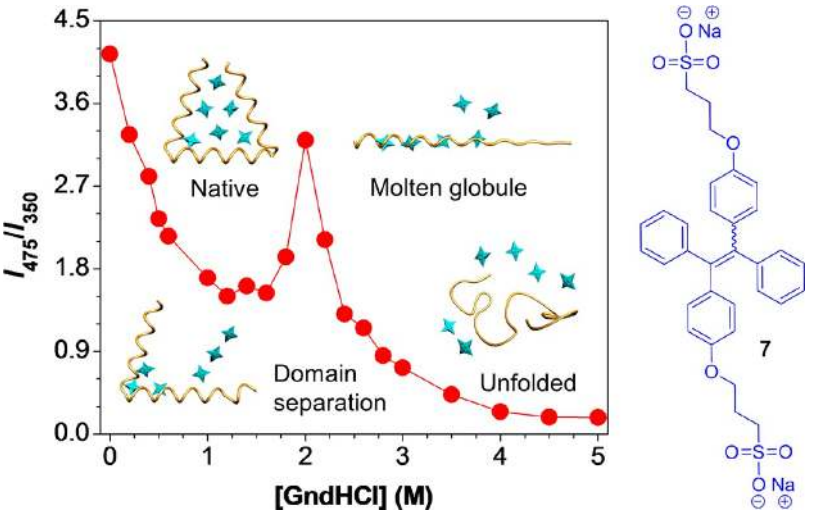

FIGURE 5. Dependence of I_{475}/I_{350} between HSA and **7** on the concentration of GdnHCl and illustration of GndHCl-induced HSA unfolding processes. Reproduced with permission from ref 18. Copyright 2010 American Chemical Society.

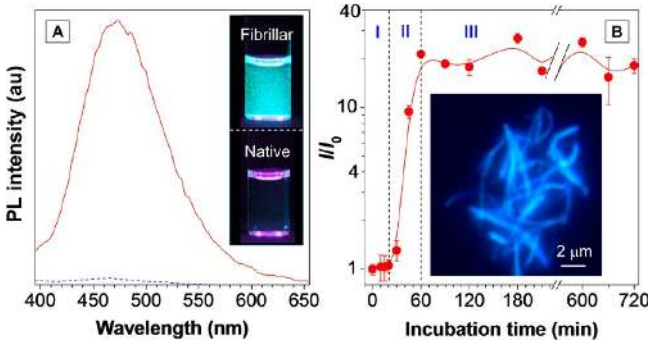

FIGURE 6. (A) Photoluminescence (PL) spectra of **7** in the presence of native (blue dashed line) and fibrillar (red solid line) forms of bovine insulin. Inset: Photographs of **7** with native and fibrillar forms of insulin taken under UV illumination. (B) Process of insulin fibrosis monitored by the fluorescence change of **7**. Inset: Fluorescence image of **7**-stained insulin fibrils. Reproduced with permission from ref 20. Copyright 2012 American Chemical Society.

process: (I) nucleation, (II) elongation, and (III) equilibrium (Figure 6B). The preformed protein plaques stained by **7** appear as blue fluorescent fibers (Figure 6B inset). Premixing **7** with insulin results in inhibition of the nucleation process to impede amyloidogenesis, due to the hydrophobic interaction between phenyl rings of **7** and hydrophobic residues of insulin which stabilizes the formed complexes.

To achieve more selective protein detection with AIE fluorogens,[21] a light-up bioprobe (**8**) for integrin $\alpha_v\beta_3$ was synthesized through conjugation of cyclic arginine-glycine-aspartic acid (cRGD) with a bisazide derivative of TPS (BATPS).[22] Opposite to the bright emission of BATPS nanoaggregates in water, **8** is water-soluble and hence nonfluorescent in aqueous media (Figure 7A). The specific binding of cRGD with integrin $\alpha_v\beta_3$ is able to activate the RIR process in **8**, and the solution fluorescence is thus increased with increasing integrin $\alpha_v\beta_3$ concentration. This allows visual recognition of integrin $\alpha_v\beta_3$ with a detection limit of 10 μg/mL. The probe shows high selectivity over DNA and other proteins (Figure 7B). Further study reveals that **8** is able to image the binding process between cRGD and integrin $\alpha_v\beta_3$ on cell membrane, which allows real-time tracking of integrin $\alpha_v\beta_3$ and identifying integrin $\alpha_v\beta_3$-positive cancer cells. The light-up nature of the AIE bioprobe circumvents the multiple washing steps required for traditional fluorescent probes in an in vitro imaging process, offering new opportunities for continuous sensing or monitoring of biological processes and events.

Real-time investigation of cell apoptosis can provide valuable insights into early diagnosis of therapeutic efficiency. Caspase-3 is a key mediator of cell apoptosis that has been an attractive target for monitoring apoptosis. Taking advantage of AIE light-up probe, a caspase probe (**9**) was synthesized by conjugation of a hydrophilic Asp-Glu-Val-Asp peptide with a hydrophobic AIE fluorogen via a lysine linker.[23] While being practically nonfluorescent in aqueous media, **9** lights up in the presence of caspase-3 or -7 within minutes, due to the effective cleavage of the peptide segment by the enzyme and the RIR of the released hydrophobic TPE cores. The probe is further proved effective in evaluating cell apoptosis induced by staurosporine, which overlaps well with the commercial anti-caspase-3 stain (panels B and C in Figure 8). Further studies show that the probe can be used to monitor cell apoptosis processes in real time, offering a superb tool for in situ screening of

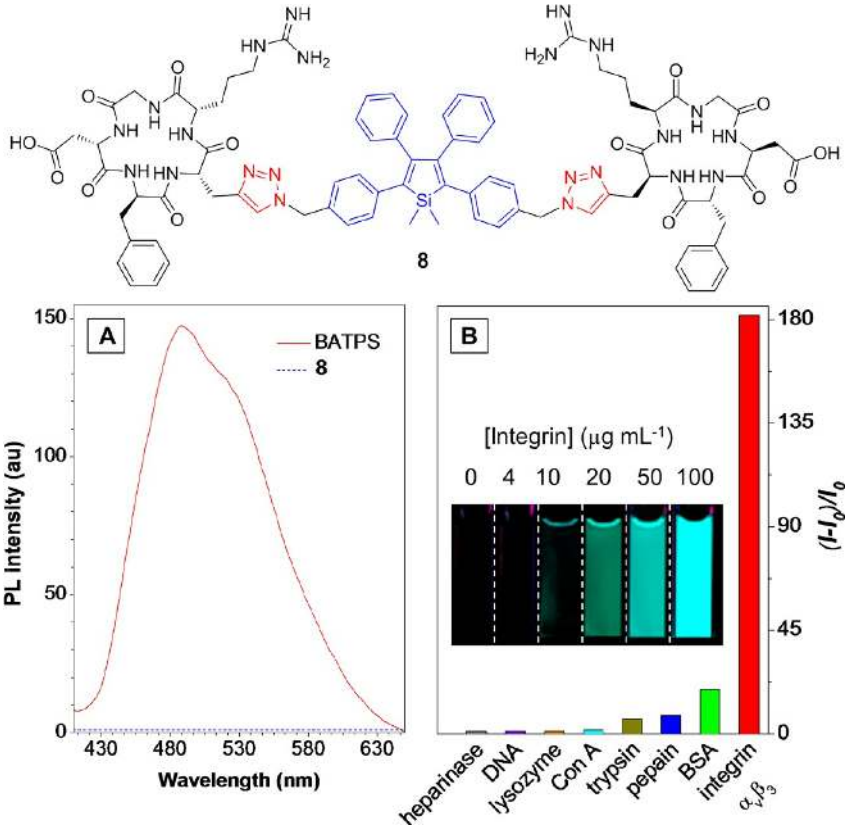

FIGURE 7. (A) PL spectra of BATPS and **8** in DMSO/water mixture. (B) Plot of $(I - I_0)/I_0$ versus different proteins and DNA, where I and I_0 are the PL intensities at analyte concentrations of 100 and 0 μg mL^{-1}, respectively. Inset: photographs taken under UV illumination for **8** in the presence of integrin $\alpha_v\beta_3$ at different concentrations. Reproduced with permission from ref 22. Copyright 2012 American Chemical Society.

enzyme inhibitors and evaluation of apoptosis-associated drug efficacy.

2.3. Sensing of Small Biomolecules. Besides DNA and proteins, many small biomolecules such as cysteine and sugars also play important roles in the complex biological processes. A maleimide-tagged TPE (**10**) was synthesized for specific thiol detection.[9] Whereas **10** is nonemissive due to the photoinduced electron transfer from TPE to maleimide unit, its thiolated adduct (**11**) shows marked AIE effect. This unique thiol−ene click reaction allows the solid spots of **10** on the TLC plates to be selectively lightened up by L-cysteine for visual detection (Figure 9B).

Boric acids can form boronate complexes with diols in aqueous media. A TPE-diboronic acid adduct (**12**) was synthesized, which is nonemissive in a carbonate buffer (pH 10.5). It lights up upon addition of 0.1 mM D-glucose (Glu) but not D-fructose (Fru), D-galactose (Gal), and D-mannose (Man), due to the folding and aggregation of the oligoboronates from oligomerization of Glu with **12** (Figure 10).[24] Based on a similar design principle, a diboronic-acid-functionalized analogue of **12** with a *cis*-configuration shows selective response to β-cyclodextrin.

3. Fluorescence Imaging

The commonly used fluorescence imaging reagents include organic dyes and proteins (e.g., green fluorescent protein), whose molar absorptivity and photobleaching resistance are, however, both low. Inorganic QDs have also been used but suffer from high cytotoxicity in oxidative environment.[9] The development of organic dots has been largely hampered by the ACQ effect involved in the conventional fluorophore systems. The high brightness of AIE fluorogens in the solid state and the distinct feature that AIE fluorogens become stronger emitters at higher concentrations make them promising candidate materials for fluorescence imaging applications.

3.1. Bare AIE Dots. Aminated silole derivatives **13** are AIE fluorogens that spontaneously aggregate into nanoscopic dots in aqueous media with an average size of ~220 nm (Figure 11A).[25] The nanodots of **13** are biocompatible with bright green fluorescence and can effectively stain HeLa cells. The strong retention of the AIE dots in the HeLa cells prevents the cocultured human embryonic kidney (HEK) 293T cells from being contaminated (Figure 11B). The good cellular retention along with high brightness of the dots has

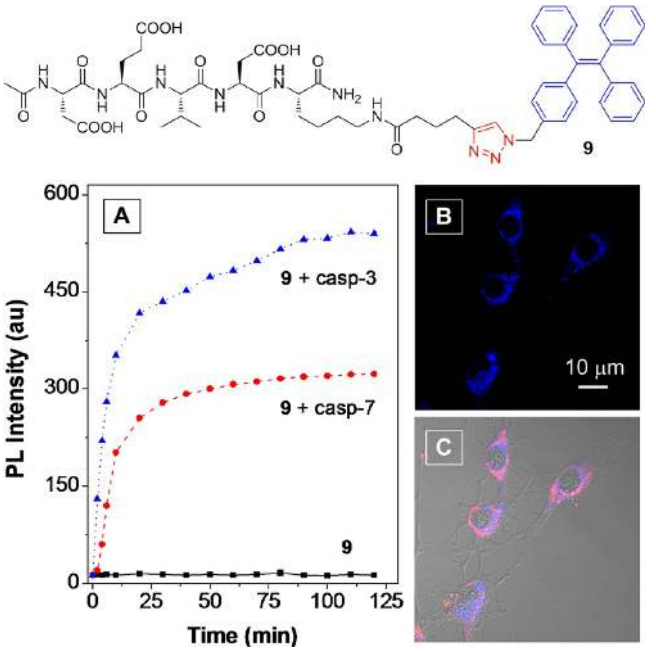

FIGURE 8. (A) Time-dependent fluorescence response of **9** to caspase-3/7. (B) Fluorescence image of staurosporine-induced apoptotic MCF-7 cells treated with **9** and (C) its overlay image with commercial anti-caspase-3 stain. Reproduced with permission from ref 23. Copyright 2012 American Chemical Society.

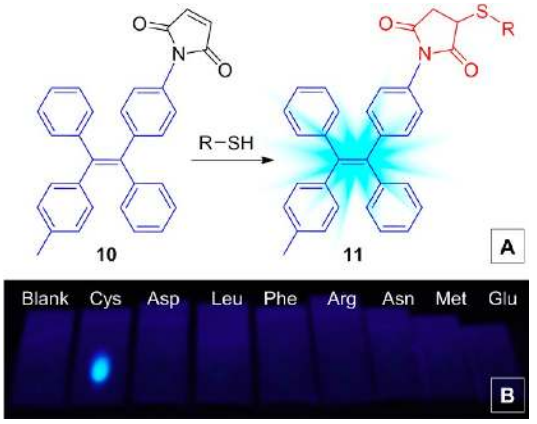

FIGURE 9. (A) Schematic illustration of **10** for thiol detection. (B) Fluorescent discrimination of cysteine from other amino acids on TLC plates. Reproduced with permission from ref 9. Copyright 2011 Royal Society of Chemistry.

enabled long-term HeLa cell tracing up to four passages (Figure 11C and D). The AIE dots outperform commercial CellTracker Green CMFDA and enable visual monitoring of the cell growth. Due to their AIE feature and charge neutrality, **13** can be used in high concentrations for cellular imaging, overcoming the problems of small molecule tracers, such as low probe concentration and short cellular retention.

3.2. Silica AIE Dots. To improve photobleaching resistance and colloidal stability of AIE dots, fluorescent silica

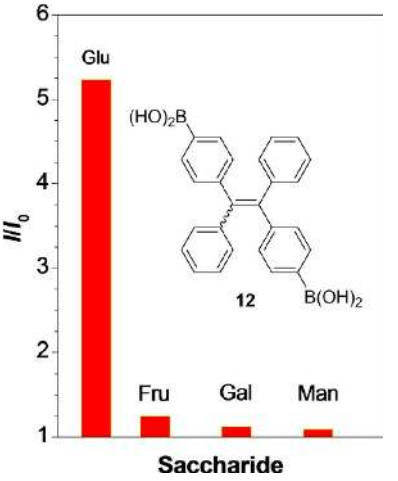

FIGURE 10. Response of **12** to different saccharides. I_0 is the intensity of **12** at pH 12.

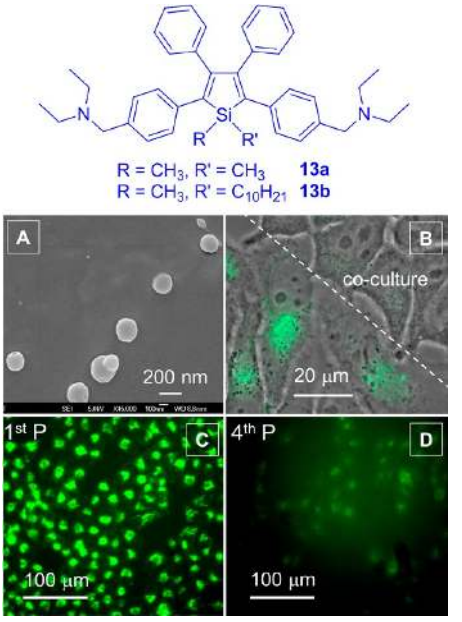

FIGURE 11. (A) SEM image of AIE dots of **13a**. (B) phase contrast and fluorescence images of **13b**-stained HeLa cells cocultured with unstained HEK 293T cells. Fluorescence images of living HeLa cells stained with **13b** at the (C) first and (D) fourth passages (P). Reproduced with permission from ref 25. Copyright 2011 Wiley-VCH.

FIGURE 12. Fabrication of **14**-cored FSDs and their TEM images.

dots (FSDs) were fabricated by incorporating AIE fluorogens into silica networks through a sol–gel approach (Figure 12).[9,26] Silica was chosen as the matrix because it is hydrophilic, biocompatible, and photostable. Starting from a triethoxysilylated TPE derivative (**14**), blue light-emitting FSDs with sizes tunable in the range of 50–300 nm were prepared. The **14**-cored FSDs show low cytotoxicity to living cells with excellent colloidal stability. In another study, a TPS derivative **15** (Figure 13) was synthesized via click chemistry and **15**-based FSDs were prepared using both Stöber and reverse microemulsion methods with uniform sizes of 220 and 60 nm, respectively.

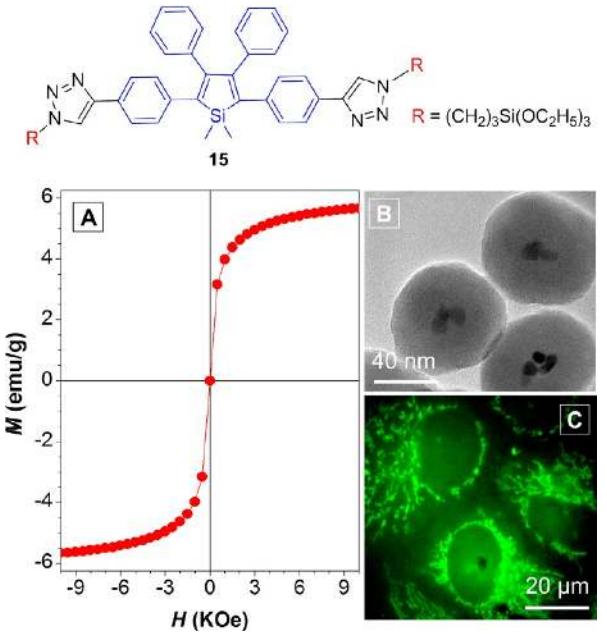

FIGURE 13. (A) Plot of magnetization (*M*) versus applied magnetic field (*H*) for **15**-based FMDs at 300 K. (B) TEM images of the dots and (C) fluorescence images of HeLa cells stained by the dots. Reproduced with permission from ref 27. Copyright 2011 Wiley-VCH.

Integration of fluorescent and magnetic components is an attractive proposition. It is, however, challenging to fabricate fluorescent and magnetic dots (FMDs), for the magnetic components often quench fluorescence of the chromophores when they are in close proximity. As **15** is in the aggregate state and a silica spacer is inserted between the layers of **15** and citrate-coated iron oxide,[27] the resultant FMDs show bright fluorescence and strong magnetization (Figure 13A). The FMDs have a magnetic core with a mean diameter of ~19 nm and a silica shell with a thickness of ~28 nm (Figure 13B), which are readily internalized by HeLa cells for cytoplasmic staining (Figure 13C). In a separate report, AIE silica nanoprobes have been used for targeted in vivo imaging.[28]

3.3. DSPE-PEG AIE Dots. A nanoprecipitation strategy was developed to fabricate AIE dots with surface targeting ligands, employing folate-functionalized 1,2-distearoyl-*sn*-glycero-3-phosphoethanolamine-*N*-poly(ethylene glycol) (DSPE-PEG_{5000}-folate) as encapsulation matrix.[29] Unlike the FSD synthesis which requires specific modification on each AIE fluorogen, this strategy enjoys general applicability. The folate density can be fine-tuned by varying the feed ratio of DSPE-PEG_{5000}-folate and DSPE-PEG_{2000} for dot preparation. As shown in Figure 14, addition of a THF

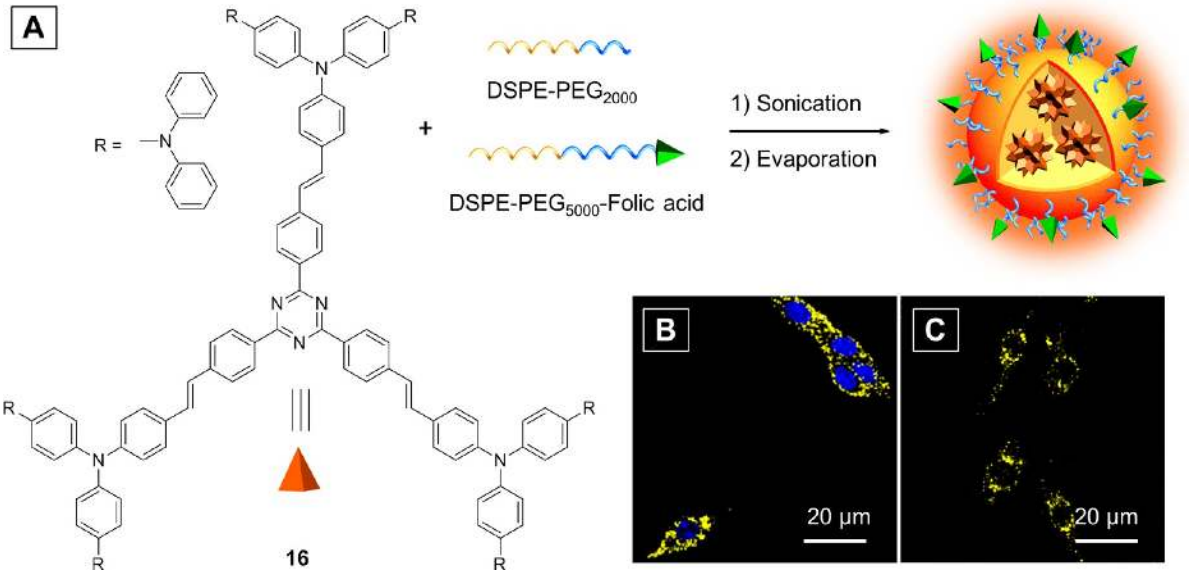

FIGURE 14. (A) Schematic illustration for the fabrication of **16**-doped DSPE-PEG-folate dots. (B) One- and (C) two-photon confocal images of MCF-7 breast cancer cells after incubation with the dots. Reproduced with permission from ref 29. Copyright 2011 Royal Society of Chemistry.

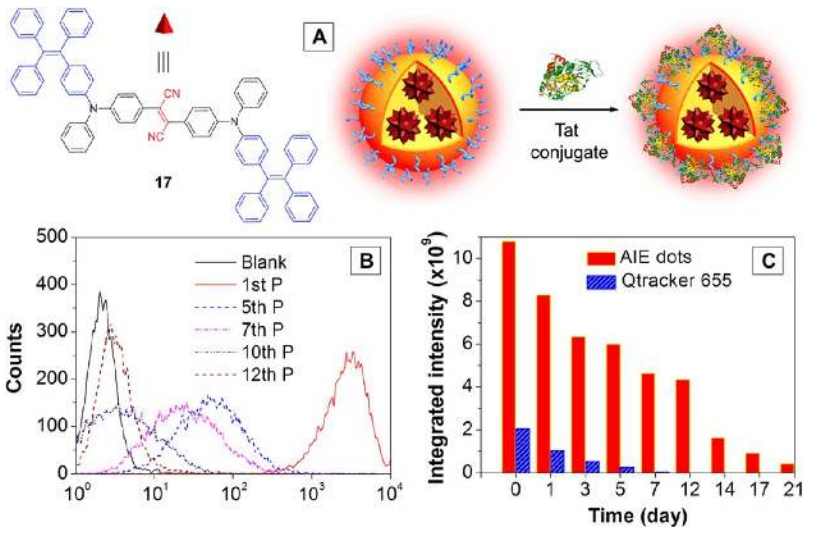

FIGURE 15. (A) Schematic illustration for the fabrication of **17**-doped DSPE-PEG-Tat dots. (B) Flow cytometry histograms of MCF-7 cells after incubation with the dots and subcultured for designated passages (P) using untreated MCF-7 cells as the blank. (C) Integrated fluorescence intensities of the tumor sites of the mouse subcutaneously injected with 1×10^6 of C6 glioma cells after staining by the dots and Qtracker 655, respectively. Reproduced with permission from ref 12. Copyright 2012 Nature Publishing Group.

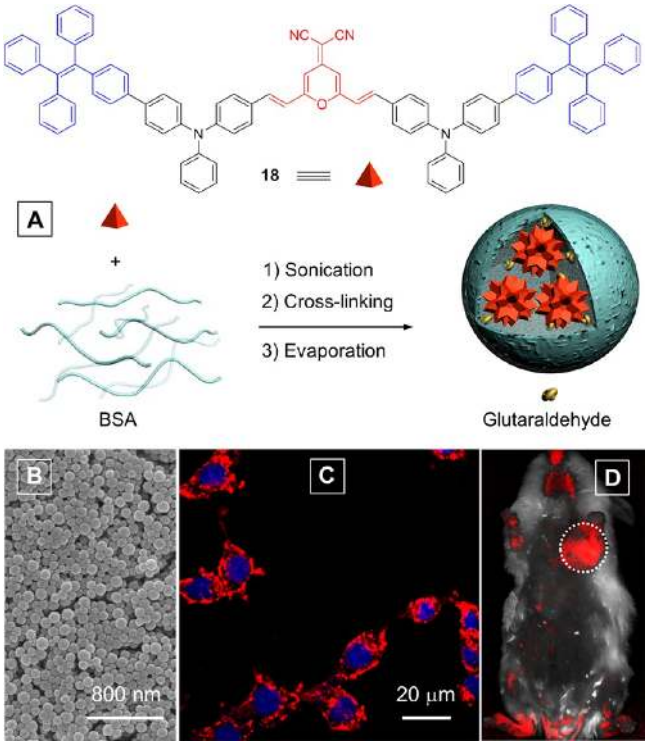

FIGURE 16. (A) Schematic illustration for the fabrication of **18**-based AIE dots and (B) their SEM image. (C) Confocal image of MCF-7 breast cancer cells after incubation with the dots. (D) In vivo noninvasive fluorescence imaging of H22 tumor-bearing mice after intravenous injection of the dots. The white circle marks the tumor site. Reproduced with permission from ref 13. Copyright 2012 Wiley-VCH.

solution of **16**, DSPE-PEG_{2000}, and DSPE-PEG_{5000}-folate into water under continuous sonication yields spherical dots with yellow emission. The dots show good selectivity between MCF-7 and NIH3T3 cells due to the suppression of nonspecific cell uptake by the PEG shell and the specific folate receptor-mediated endocytosis for MCF-7 cells. The dots are suitable for two-photon excited fluorescence (TPEF) imaging due to their large molecular two-photon absorbing (TPA) cross section (σ = 2015 GM) at 800 nm. The dots are superior to most water-soluble TPA chromophores which show very small σ values in water.[29] In comparison to one-photon excited fluorescence imaging, TPEF imaging is advantageous in terms of minimizing autofluorescence from biological tissues and increasing penetration depth.

Using the similar strategy, dots of TPE-DDPD (Figure 1) were fabricated to show bright FR/NIR fluorescence for in vitro and in vivo targeted tumor cell imaging.[11] The cellular uptake of the DSPE-PEG-folate encapsulated dots by MCF-7 cells was found to be mainly via caveolae-mediated but not clathrin-mediated endocytosis, and macropinocytosis was not involved in the uptake process.[30]

Furthermore, a two-step synthetic strategy was developed for the preparation of AIE dots with surface functional groups.[12,31,32] For instance, DSPE-PEG_{2000} and DSPE-PEG_{2000}-NH_2 were used to coencapsulate fluorogen **17**, which was synthesized by conjugating TPE with 2,3-bis-[4-(diphenylamino)phenyl]fumaronitrile (TPAFN). As TPAFN is AIE active, the molecular fusion of the two types of AIE units (AIE + AIE) yielded a new fluorogen (**17**) with extended electronic conjugation, long absorption wavelength, and large molar absorptivity. The **17**-based AIE dots show a

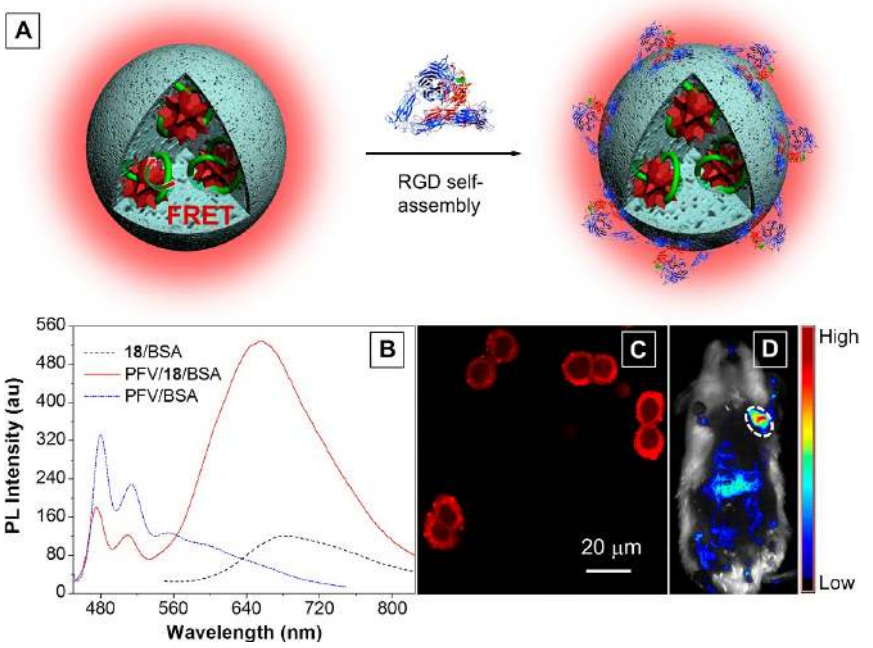

FIGURE 17. (A) Schematic illustration of RGD functionalization of PFV/**18** coloaded BSA dots. (B) PL spectra of different dots in water. (C) Confocal laser scanning microscopy images of HT-29 cancer cells incubated with the dots. (D) In vivo noninvasive fluorescence imaging of H22 tumor-bearing mice after intravenous injection of the dots. The white circle indicates the tumor site. Reproduced with permission from ref 33. Copyright 2012 Wiley-VCH.

uniform hydrodynamic size of 30 nm, an emission maximum of 671 nm, and a quantum yield of 24%. Further functionalization of the dots with HIV-1 transactivator of transcription (Tat) via carbodiimide-mediated coupling (Figure 15A) affords **17**-doped DSPE-PEG-Tat dots. On average, each Tat-AIE dot is over 1 order of magnitude brighter than the commercial Qtracker 655 and the notorious blinking behavior of QDs is absent in the Tat-AIE dots. Noninvasive cell tracing experiments show that the AIE-dots and QDs are capable of tracing MCF-7 cells for 10−12 and 5−6 generations in vitro (Figure 15B), and continuous monitoring C6 glioma cells in mice up to 21 days and 6−7 days in vivo (Figure 15C), respectively. As **17** is also two-photon active, its large σ value (6.7×10^5 GM) at 810 nm enables deep TPEF imaging of tumors up to 550 μm. The outstanding performance of the Tat-AIE dots opens a new avenue in the development of advanced fluorescent probes for monitoring biological processes.

3.4. BSA AIE Dots. Besides the synthetic DSPE-PEG matrix, bovine serum albumin (BSA), a protein with wide clinical applications, has also been demonstrated effective as an AIE fluorogen-encapsulating matrix.[13] For example, **18** was prepared by attaching two TPE units to the ends of 2-{2,6-bis[(*E*)-4-(diphenylamino)styryl]-4*H*-pyran-4-ylidene}-malononitrile (TPA-DCM; Figure 16). TPA-DCM is a well-known red emitter but not so emissive in polar solvent and solid state due to the TICT and ACQ processes, respectively. As TICT is one of the most popular strategies to realize long wavelength emission with optical nonlinearity, the AIE + TICT strategy that successfully transforms TPA-DCM into AIE-active **18** represents a new molecular design strategy to realize bright FR/NIR dots for TPEF imaging.

The schematic illustration for the fabrication of **18**-loaded BSA dots is shown in Figure 16A. Addition of **18** in THF to BSA aqueous solution under sonication followed by cross-linking with glutaraldehyde affords **18**-loaded BSA dots with an emission maximum of 668 nm and a uniform size of ~100 nm (Figure 16B). Incubation with MCF-7 cells reveals that the dots can function as effective visualizers for intracellular imaging (Figure 16C). In vivo bioimaging with **18**-loaded BSA dots shows preferential accumulation in tumor tissue, due to the enhanced permeability and retention effect of the dots with a diameter of 100 nm.

The fluorescence of the **18**-loaded BSA dots can be further intensified by over 5-fold via FRET from poly(9,9-bis{2-[2-(2-methoxyethoxy)ethoxy]ethyl}fluorenyldivinylene) (PFV) upon coencapsulation into BSA (Figure 17).[33] As BSA surface is negatively charged in water, further self-assembly between the dots and RGD peptide generates PFV/**18** coloaded BSA-RGD dots, which can specifically recognize

integrin receptor-overexpressed cancer cells both in vitro and in vivo with high contrast (Figure 17 C and D).

4. Conclusions

This Account summarizes our recent work on the development of fluorescent bioprobes based on AIE fluorogens whose fluorescence is weak as isolated molecules but strong in aggregate state. Stating from simple rotors (e.g., TPE and TPS), the AIE units work like magic sticks that can conjugate with a variety of molecular blocks (e.g., ACQ, AIE, and TICT units) to enrich the family of AIE fluorogens with emission tunable from blue to NIR and efficiency up to unity as aggregates.

The AIE effect permits the use of highly concentrated solutions of fluorogens as well as their nanoaggregates for biosensor applications. Ionic AIE fluorogens are able to respond to different DNA structures with good sensitivity. Conjugation of AIE fluorogens with bioreceptors leads to light-up probes for specific analyte detection. In comparison to the fluorescence turn-off probes based on conventional ACQ dyes, the turn-on nature of the AIE probes offers higher sensitivity and better accuracy and allows direct visualization of biological analytes and processes in aqueous media. The bright nanoaggregates of AIE fluorogens offer new opportunities for tumor cell detection and imaging. The AIE probe performances have been further enhanced via particle formulation and surface functionalization, showing advanced features over inorganic QDs and organic dyes in terms of brightness, biocompatibility, and cellular retention.

Further development of AIE fluorogen-based bioprobes will be focused on FR/NIR emitters, especially those obtained via TICT + AIE strategy, which will pave the way to the development of new multiphoton fluorescence materials for theranostic applications.[34] In addition, molecular engineering of new AIE fluorogens with more specific receptors will create light-up bioprobes with improved sensitivity and selectivity to bioanalytes. Considering that the RIR process plays an essential role in bioluminescence systems (e.g., green fluorescent proteins), the bioprobes demonstrated in this Account are expect to stimulate new exciting research and to promote AIE fluorogens as practical tools in biological world.

We thank IMRE (11-1C0213), NRF of Singapore (R279-000-323/390-281), RGC of Hong Kong (HKUST2/CRF/10 and AoE/P-03/08), National Basic Research Program of the Ministry of Science & Technology of China (973 Program; 2013CB834701), and Guangdong Innovative Research Team Program (201101C0105067115) for financial support.

Note Added after ASAP Publication. This paper posted to the Web on June 6, 2013. Chart 1 was corrected and the revised version was reposted on June 10, 2013.

BIOGRAPHICAL INFORMATION

Dan Ding received his Ph.D. degree from Nanjing University. He is currently a research fellow at National University of Singapore (NUS) under the supervision of Prof. Liu. His research focuses on fluorescent nanomaterials for bioimaging.

Kai Li received his Ph.D. degree from NUS under the supervision of Prof. Liu. He is currently a research scientist at Institute of Materials Research and Engineering, Singapore. His research focuses on organic nanoparticles for biosensor applications.

Bin Liu received her Ph.D. degree from NUS and conducted her postdoctoral work at University of California, Santa Barbara. She is currently an Associate Professor in the Department of Chemical and Biomolecular Engineering of NUS. She works on conjugated polyelectrolytes and organic nanoparticles for biological applications.

Ben Zhong Tang received his Ph.D. degree from Kyoto University and conducted his postdoctoral work at University of Toronto. He is Stephen K. C. Cheong Professor of Science at HKUST and Associate Editor of *Polymer Chemistry*. He is interested in creating new molecules with novel structures and unique properties. He was elected to Chinese Academy of Sciences in 2009.

FOOTNOTES

*To whom correspondence should be addressed. E-mail: cheliub@nus.edu.sg (B.L.); tangbenz@ust.hk (B.Z.T.).
The authors declare no competing financial interest.

REFERENCES

1 Haugland, R. P. *The Molecular Probes Handbook: A Guide to Fluorescent Probes and Labeling Technologies*; Life Technologies: Carlsbad, CA, 2010.
2 Birks, J. B. *Photophysics of Aromatic Molecules*; Wiley: New York, 1970.
3 Zhelev, Z.; Ohba, H.; Bakalova, R. Single Quantum Dot-Micelles Coated with Silica Shell as Potentially Non-Cytotoxic Fluorescent Cell Tracers. *J. Am. Chem. Soc.* **2006**, *128*, 6324–6325.
4 Valeur, B. *Molecular Fluorescence: Principle and Applications*; Wiley-VCH: Weinheim, 2002.
5 Borisov, S. M.; Wolfbeis, O. S. Optical Biosensors. *Chem. Rev.* **2008**, *108*, 423–461.
6 Hong, Y.; Lam, J. W. Y.; Tang, B. Z. Aggregation-Induced Emission: Phenomenon, Mechanism and Applications. *Chem. Commun.* **2009**, 4332–4353.
7 Luo, J.; Xie, Z.; Lam, J. W. Y.; Cheng, L.; Chen, H.; Qiu, C.; Kwok, H. S.; Zhan, X.; Liu, Y.; Zhu, D.; Tang, B. Z. Aggregation-Induced Emission of 1-Methyl-1,2,3,4,5-Pentaphenylsilole. *Chem. Commun.* **2001**, *18*, 1740–1741.
8 Peng, Q.; Yi, Y.; Shuai, Z.; Shao, J. Toward Quantitative Prediction of Molecular Fluorescence Quantum Efficiency: Role of Duschinsky Rotation. *J. Am. Chem. Soc.* **2007**, *129*, 9333–9339.
9 Hong, Y.; Lam, J. W. Y.; Tang, B. Z. Aggregation-Induced Emission. *Chem. Soc. Rev.* **2011**, *40*, 5361–5388.
10 Wang, M.; Zhang, G.; Zhang, D.; Zhu, D.; Tang, B. Z. Fluorescent Biochemosensors Based on Silole and Tetraphenylethene Luminogens with Aggregation-induced Emission Feature. *J. Mater. Chem.* **2010**, *20*, 1858–1867.
11 Zhao, Q.; Li, K.; Chen, S.; Qin, A.; Ding, D.; Zhang, S.; Liu, Y.; Liu, B.; Sun, J. Z.; Tang, B. Z. Aggregation-Induced Red-NIR Emission Organic Nanoparticles as Effective and Photostable Fluorescent Probes for Bioimaging. *J. Mater. Chem.* **2012**, *22*, 15128–15135.
12 Li, K.; Qin, W.; Ding, D.; Geng, J.; Liu, J.; Zhang, X.; Liu, H.; Liu, B.; Tang, B. Z. Photostable Fluorescent Organic Dots with Aggregation-Induced Emission (AIE Dots) for Noninvasive Long-Term Cell Tracing. *Sci. Rep.* **2013**, *3*, 1150.

13 Qin, W.; Ding, D.; Liu, J.; Yuan, W. Z.; Hu, Y.; Liu, B.; Tang, B. Z. Biocompatible Nanoparticles with Aggregation-Induced Emission Characteristics as Far-Red/Near-Infrared Fluorescent Bioprobes for in Vitro and in Vivo Imaging Applications. *Adv. Funct. Mater.* **2012**, *22*, 771–779.

14 Zhang, G. F.; Aldred, M. P.; Gong, W. L.; Li, C.; Zhu, M. Q. Utilising Tetraphenylethene as a Dual Activator for Intramolecular Charge Transfer and Aggregation Induced Emission. *Chem. Commun.* **2012**, *48*, 7711–7713.

15 Hong, Y.; Xiong, H.; Lam, J. W. Y.; Häußler, M.; Liu, J.; Yu, Y.; Zhong, Y.; Sung, H.; Williams, I. D.; Wong, K. S.; Tang, B. Z. Fluorescent Bioprobe: Structural Matching in the Docking Process of Aggregation-Induced emission Fluorogens on DNA Surfaces. *Chem.—Eur. J.* **2010**, *16*, 1232–1245.

16 Xu, X.; Li, J.; Li, Q.; Huang, J.; Dong, Y.; Hong, Y.; Yan, J.; Qin, J.; Li, Z.; Tang, B. Z. A Strategy for Dramatically Enhancing the Selectivity of Molecules Showing Aggregation-Induced Emission towards Biomacromolecules with the Aid of Graphene Oxide. *Chem.—Eur. J.* **2012**, *18*, 7278–7286.

17 Yu, Y.; Liu, J.; Zhao, Z.; Ng, K. M.; Luo, K. Q.; Tang, B. Z. Facile Preparation of Non-Self-Quenching Fluorescent DNA Strands with the Degree of Labeling up to the Theoretic Limit. *Chem. Commun.* **2012**, *48*, 6360–6362.

18 Hong, Y.; Feng, C.; Yu, Y.; Liu, J.; Lam, J. W. Y.; Luo, K. Q.; Tang, B. Z. Quantitation, Visualization and Monitoring of Conformational Transitions of Human Serum Albumin by a Tetraphenylethene Derivative with Aggregation-Induced Emission Characteristics. *Anal. Chem.* **2010**, *82*, 7035–7043.

19 Wang, F.; Wen, J.; Huang, L.; Huang, J.; Ouyang, J. A Highly Sensitive "Switch-on" Fluorescent Probe for Protein Quantification and Visualization Based on Aggregation-induced Emission. *Chem. Commun.* **2012**, *48*, 7395–7397.

20 Hong, Y.; Meng, L.; Chen, S.; Leung, C. W. T.; Da, L.-T.; Faisal, M.; Silva, D.-A.; Liu, J.; Lam, J. W. Y.; Huang, X.; Tang, B. Z. Monitoring and Inhibition of Insulin Fibrillation by a Small Organic Fluorogen with Aggregation-Induced Emission Characteristics. *J. Am. Chem. Soc.* **2012**, *134*, 1680–1689.

21 Sanji, T.; Shiraishi, K.; Nakamura, M.; Tanaka, M. Fluorescence Turn-on Sensing of Lectins with Mannose-substituted Tetraphenylethenes Based on Aggregation-induced Emission. *Chem.—Asian J.* **2010**, *5*, 817–824.

22 Shi, H.; Liu, J.; Geng, J.; Tang, B. Z.; Liu, B. Specific Detection of Integrin $\alpha_v\beta_3$ by Light-up Bioprobe with Aggregation-Induced Emission Characteristics. *J. Am. Chem. Soc.* **2012**, *134*, 9569–9572.

23 Shi, H.; Kwok, R. T. K.; Liu, J.; Xing, B.; Tang, B. Z.; Liu, B. Real-Time Monitoring of Cell Apoptosis and Drug Screening Using Fluorescent Light-up Probe with Aggregation-Induced Emission Characteristics. *J. Am. Chem. Soc.* **2012**, *134*, 17972–17981.

24 Liu, Y.; Deng, C.; Tang, L.; Qin, A.; Hu, R.; Sun, J. Z.; Tang, B. Z. Specific Detection of D-Glucose by a Tetraphenylethene-Based Fluorescent Sensor. *J. Am. Chem. Soc.* **2011**, *133*, 660–663.

25 Yu, Y.; Feng, C.; Hong, Y. N.; Liu, J. Z.; Chen, S. J.; Ng, K. M.; Luo, K. Q.; Tang, B. Z. Cytophilic Fluorescent Bioprobes for Long-Term Cell Tracking. *Adv. Mater.* **2011**, *23*, 3298–3302.

26 Kim, S.; Pudavar, H. E.; Bonoiu, A.; Prasad, P. N. Aggregation-enhanced Fluorescence in Organically Modified Silica Nanoparticles: A Novel Approach toward High-signal-output Nanoprobes for Two-photon Fluorescence Bioimaging. *Adv. Mater.* **2007**, *19*, 3791–3795.

27 Faisal, M.; Yu, Y.; Lam, J. W. Y.; Liu, J.; Zhang, B.; Lu, P.; Zhang, X.; Tang, B. Z. Fabrication of Silica Nanoparticles with both Efficient Fluorescence and Strong Magnetization, and Exploration of Their Biological Applications. *Adv. Funct. Mater.* **2011**, *21*, 1733–1740.

28 Wang, X.; Morales, A. R.; Urakami, T.; Zhang, L.; Bondar, M. V.; Komatsu, M.; Belfield, K. D. Folate Receptor-targeted Aggregation-enhanced Near-IR Emitting Silica Nanoprobe for One-photon in Vivo and Two-photon ex Vivo Fluorescence Bioimaging. *Bioconjugate Chem.* **2011**, *22*, 1438–1450.

29 Li, K.; Jiang, Y. H.; Ding, D.; Zhang, X.; Liu, Y. T.; Hua, J. L.; Feng, S. S.; Liu, B. Folic Acid-Functionalized Two-Photon Absorbing Nanoparticles for Targeted MCF-7 Cancer Cell Imaging. *Chem. Commun.* **2011**, *47*, 7323–7325.

30 Geng, J. L.; Li, K.; Ding, D.; Zhang, X. H.; Qin, W.; Liu, J. Z.; Tang, B. Z.; Liu, B. Lipid-PEG-Folate Encapsulated Nanoparticles with Aggregation Induced Emission Characteristics: Cellular Uptake Mechanism and Two-Photon Fluorescence Imaging. *Small* **2012**, *8*, 3655–3663.

31 Yang, Y.; An, F.; Liu, Z.; Zhang, X.; Zhou, M.; Li, W.; Hao, X.; Lee, C.; Zhang, X. Ultrabright and Ultrastable Near-infrared Dye Nanoparticles. *Biomaterials* **2012**, *33*, 7803–7809.

32 Wang, D.; Qian, J.; He, S. L.; Park, J. S.; Lee, K. S.; Han, S. H.; Mu, Y. Aggregation—enhanced Fluorescence in PEGylated Phospholipid Nanomicelles for in vivo Imaging. *Biomaterials* **2011**, *32*, 5880–5888.

33 Ding, D.; Li, K.; Qin, W.; Zhan, R. Y.; Hu, Y.; Liu, J. Z.; Tang, B. Z.; Liu, B. Conjugated Polymer Amplified Far-Red/Near-Infrared Fluorescence from Nanoparticles with Aggregation-Induced Emission Characteristics for Targeted in Vivo Imaging. *Adv. Healthcare Mater.* **2013**, *2*, 500–507.

34 Chang, C. C.; Hsieh, M. C.; Lin, J. C.; Chang, T. C. Selective Photodynamic Therapy Based on Aggregation-induced Emission Enhancement of Fluorescent Organic Nanoparticles. *Biomaterials* **2012**, *33*, 897–906.